Linearly Polarized Modes of a Corrugated Metallic Waveguide

Elizabeth J. Kowalski, *Student Member, IEEE*, David S. Tax, *Student Member, IEEE*, Michael A. Shapiro, *Member, IEEE*, Jagadishwar R. Sirigiri, *Member, IEEE*, Richard J. Temkin, *Fellow, IEEE*, Timothy S. Bigelow, and David A. Rasmussen

***Abstract*—A linearly polarized (LP_{mn}) mode basis set for oversized, corrugated, metallic waveguides is derived for the special case of quarter-wavelength-depth circumferential corrugations. The relationship between the LP_{mn} modes and the conventional modes $(\mathrm{HE}_{mn}, \mathrm{EH}_{mn}, \mathrm{TE}_{0n}, \mathrm{TM}_{0n})$ of the corrugated guide is shown. The loss in a gap or equivalent miter bend in the waveguide is calculated for single-mode and multimode propagation on the line. In the latter case, it is shown that modes of the same symmetry interfere with one another, causing enhanced or reduced loss, depending on the relative phase of the modes. If two modes with azimuthal (m) indexes that differ by one propagate in the waveguide, the resultant centroid and the tilt angle of radiation at the guide end are shown to be related through a constant of the motion. These results describe the propagation of high-power linearly polarized radiation in overmoded corrugated waveguides.**

***Index Terms*—Corrugated waveguide, linearly polarized modes, miter bends, oversized waveguide.**

I. Introduction

An important problem in research with high-power, high-frequency coherent microwave radiation is the transmission of the radiation from the source of power to its application. Recently, rapid advances in the development of gyrotrons have made sources of continuous power available at levels in the megawatt range at frequencies of up to 170 GHz. The radiation from gyrotrons is often transported long distances, many tens of meters, before being launched for plasma heating. The transmission lines ordinarily used in these applications are oversized corrugated metallic waveguides. These waveguides provide low loss and low mode conversion. The metallic wall prevents some loss of radiation. Other major uses of these corrugated waveguides include transmission lines for plasma diagnostics, radar, materials heating, and spectroscopy.

Manuscript received May 14, 2010; revised August 04, 2010; accepted August 16, 2010. Date of publication October 07, 2010; date of current version November 12, 2010. This work was supported in part by the U.S. Department of Energy (DOE) Office of Fusion Energy Sciences, the U.S. DOE Virtual Laboratory for Technology and the U.S. ITER Project managed by Battelle/Oak Ridge National Laboratory.

E. J. Kowalski, D. S. Tax, M. A. Shapiro, J. R. Sirigiri, and R. J. Temkin are with the Plasma Science and Fusion Center, Massachusetts Institute of Technology, Cambridge, MA 02139 USA (e-mail: ejk@mit.edu; dtax@mit.edu; shapiro@psfc.mit.edu; jsirigiri@bridge12.com; temkin@mit.edu).

T. S. Bigelow and D. A. Rasmussen are with the U.S. ITER Project Office and Oak Ridge National Laboratory, Oak Ridge, TN 37831 USA (e-mail: bigelowts@ornl.gov; rassummenda@ornl.gov).

Color versions of one or more of the figures in this paper are available online at http://ieeexplore.ieee.org.

Digital Object Identifier 10.1109/TMTT.2010.2078972

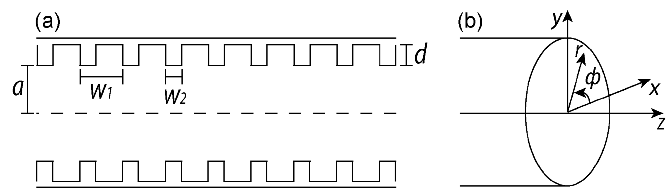

Fig. 1. (a) Cylindrical circumferentially corrugated waveguide with a radius of a. The corrugations are defined by w_1, w_2, and d. For low-loss characteristics, the corrugation depth is $d = \lambda/4$. (b) Illustration of the variables in the cylindrical geometry.

Corrugated waveguides consist of hollow metallic cylinders where the inner wall has periodic wavelength-scaled grooves, as depicted in Fig. 1. Fig. 1 also shows the parameters of the waveguide and the coordinates used in describing the modes. The fundamental mode of the corrugated waveguide, the HE_{11} mode, has less attenuation than the fundamental modes for equivalent smooth-wall cylindrical and rectangular waveguides. This effect is reviewed for frequencies from 1 to 10 GHz in [1] and for the 100-GHz range in [2]. Overmoded corrugated waveguides have extremely low losses at high frequencies, even for higher order modes [3], [4]. The attenuation for a corrugated guide scales inversely with the cube of the radius to wavelength ratio, a/λ. Therefore, attenuation in an oversized waveguide is so low that we will omit discussion of that loss in this paper; the loss is discussed at length in [5].

Originally, corrugated waveguides were developed tangentially for horn antennas, but recent applications for straight corrugated waveguides have led to a great deal of literature devoted to oversized corrugated waveguides. The theory for modes of corrugated metallic waveguides has been previously developed [1], [2], [6], [7]. A set of eigenmodes, a basis set of solutions to Maxwell's equations in corrugated waveguide, has been derived for corrugated metallic waveguides consisting of hybrid modes, both HE_{mn} and EH_{mn} modes, plus the TE_{0n} and TM_{0n} modes [5], [8], [9].

The results obtained in this paper are for the case of a quarter-wavelength groove depth, $d = \lambda/4$, which is the optimum depth for the lowest attenuation in the waveguide. The corrugation period w_1 is $\lambda/3$. We will also specialize our analysis to waveguides with large values of a/λ. An important application that is currently under development is the transmission line for the electron cyclotron heating system for the ITER tokamak, which will have 24 1-MW gyrotrons at 170 GHz. Each gyrotron will have a transmission line that is over 100 m long [10]. These transmission lines have been designed with a corrugation depth $d = \lambda/4$ of 0.44 mm and a radius of $a =$ 31.75 mm, such that

$a/\lambda = 18$ [11]. In this paper, we will use this case for illustrating some important examples.

Overmoded corrugated waveguides ideally operate only in the fundamental HE_{11} mode, but higher order modes also propagate along the line with low losses. For many high-power, high-frequency experiments, such as ITER, gyrotrons are used to produce Gaussian (TEM_{00}) beam inputs for the transmission-line system. Ideally, the Gaussian beam couples to and propagates as the fundamental HE_{11} mode in the transmission line, with 98% theoretical coupling [12]. However, experimental gyrotron inputs are imperfect Gaussian beams and can be injected into the transmission-line system with tilt and/or offset, causing the excitation of higher order modes on the overmoded transmission line [13]. These higher order modes are supported in the line and will propagate with small attenuation. Interference effects caused by higher order modes, that is, by the presence of more than one mode on the transmission line, are considered in this paper. The fundamental mode of quarter-wavelength corrugated waveguide, the HE_{11} mode, is linearly polarized. However, the hybrid modes are, in general, not linearly polarized.

The purpose of this paper is to develop a set of linearly polarized eigenmodes (LP_{mn}) for corrugated metallic waveguides and calculate the effects of higher order modes on the fundamental mode. Since gyrotron beams are linearly polarized, the LP_{mn} mode set has advantages for describing this radiation. The derivation of the LP_{mn} modes is complete, but takes advantage of prior work in deriving the hybrid modes. The relationship between the LP_{mn} modes to the usual hybrid mode set is illustrated by the construction of the lowest order LP_{mn} modes, including the LP_{11} and the LP_{21} modes, from the hybrid modes. The loss in power of a single LP_{mn} mode propagating through a gap in the waveguide is derived, and the result is also analogous to the loss due to a miter bend, which is a common transmission-line component. We discuss the gap loss for a mixture of LP_{mn} modes, and, for modes of the same azimuthal symmetry, the relative phase between the modes is found to play a major role in the gap loss. For completeness, we consider two modes propagating together on the transmission line that is terminated. In this case, we find that modes of different symmetry interfere at the end of the waveguide, causing the centroid of power to be offset and/or the fields to radiate with a tilt angle. A constant of the motion involving the tilt and offset is derived.

The results derived in this paper should be useful in planning corrugated waveguide transmission lines for high-power microwave systems and in analyzing the properties of the waveguides.

II. Description of LP_{mn} Modes

Here, we show that linearly polarized LP_{mn} modes form a basis set for metallic corrugated waveguides with corrugations of depth $d = \lambda/4$. These modes are particularly convenient for use in treating the transmission of high-power radiation from gyrotrons, since gyrotrons produce linearly polarized microwave beams. We also will show the relationship of the LP_{mn}-mode basis set to the conventional hybrid-mode basis set of HE, EH, TE, and TM modes [5], [8], [9], [14]–[16]. The fields of the hybrid modes in overmoded corrugated circular waveguides are defined readily in the literature in cylindrical coordinates [5], [13]. Though the hybrid modes create a basis set, LP modes ensure proper polarization of the mode contents for common applications that use a linearly polarized gyrotron input. Since LP modes form a basis set, they may also be used to construct other beams as well, which is a necessity when considering imperfections of the input that can cause elliptically polarized modes in much smaller quantities.

The field in a corrugated waveguide can be split into two parts, the field of the propagating modes that exists for $r < a$ and the field that exists in the corrugation grooves where $a < r < a + d$. In the grooves, a standing wave pattern forms which imposes a wall impedance on the boundary $r = a$ for the propagating wave that exists at $r < a$. Within the corrugation, at $r = a + d$, $E_z = 0$ and H_ϕ is maximized. These conditions lead to the wall impedance in the z-direction as

$$Z_z = \frac{E_z(r = a)}{H_\phi(r = a)} = Z_0 \tan(kd) \tag{1}$$

where k is the wavenumber and Z_0 is defined by the corrugation widths

$$Z_0 = -j\frac{w_1 - w_2}{w_1}\sqrt{\frac{\mu_0}{\varepsilon_0}} \tag{2}$$

(see Fig. 1 for parameter definitions) [5], [8]. For the case considered here, $d = \lambda/4$, so $Z_z = \infty$, and $H_\phi(r = a) = 0$. This condition extends to the transverse electric field components, such that $E_\phi(r = a) = 0$ and $E_r(r = a) = 0$.

To satisfy the linearly polarized field stipulation, the transverse electric field for $r < a$ is expressed in Cartesian coordinates. Through coordinate definitions

$$E_y = E_r \sin\phi + E_\phi \cos\phi. \tag{3}$$

$$E_x = E_r \cos\phi - E_\phi \sin\phi. \tag{4}$$

To polarize in the $\hat{y}$-direction, E_x must be zero, which implies that $E_r = f(r, \phi, z)\sin\phi$, and $E_\phi = f(r, \phi, z)\cos\phi$. These forms satisfy the wave equations for cylindrical coordinates and boundary conditions imposed by the corrugations, as long as $f(a, \phi, z) = 0$. Therefore, $E_y = f(r, \phi, z)$ and the boundary condition that must be satisfied for linearly polarized modes is $E_y(r = a, \phi, z) = 0$. This extrapolation of E_y is similar to the definition of LP modes for dielectric waveguides, as in [17]. One main difference between the two different waveguides is the boundary conditions; whereas dielectric guides have finite fields at the wall, the metallic guides considered here have $E_y = 0$ at the wall of the guide.

Solving for the fields in the waveguide requires E_y to satisfy the wave equation as well. Though the electric field is discussed in Cartesian coordinates to satisfy the linearly polarized condition, it is more convenient to use cylindrical variables to express the function, such that

$$\frac{\partial^2 E_y}{\partial r^2} + \frac{1}{r}\frac{\partial E_y}{\partial r} + \frac{1}{r^2}\frac{\partial^2 E_y}{\partial \phi^2} + \frac{\partial^2 E_y}{\partial z^2} + \frac{\omega^2}{c^2}E_y = 0. \tag{5}$$

Assuming a z-dependence of $e^{-jk_z z}$ and a ϕ-dependence of $\cos(m\phi)$ or $\sin(m\phi)$, the wave equation is reduced to

$$r^2\frac{\partial^2 E_y}{\partial r^2} + r\frac{\partial E_y}{\partial r} + \left((k_r r)^2 - m^2\right)E_y = 0 \tag{6}$$

which is the Bessel function differential equation, where $k_r = \sqrt{(\omega^2/c^2 - k_z^2)}$. The Bessel function of the first kind is chosen to satisfy finite electric field conditions, such that

$$E_y(r,\phi,z,t) = AJ_m(k_r r)e^{j(\omega t - k_z z)}\begin{Bmatrix}\cos(m\phi)\\ \sin(m\phi)\end{Bmatrix} \quad (7)$$

where A is a constant and either sinusoidal dependence on ϕ is possible. The boundary condition $E_y(a,\phi,z) = 0$ requires that $k_r = X_{mn}/a$, where X_{mn} is the nth zero of the mth Bessel function. Through Maxwell's equations, the dominant field components for LP_{mn} modes are

$$E_{y,mn}(r,\phi) = AJ_m\left(\frac{X_{mn}r}{a}\right)\begin{Bmatrix}\cos(m\phi)\\ \sin(m\phi)\end{Bmatrix}, \quad (8)$$

$$H_{x,mn}(r,\phi) = \frac{-Ak_z}{\omega\mu_0}J_m\left(\frac{X_{mn}r}{a}\right)\begin{Bmatrix}\cos(m\phi)\\ \sin(m\phi)\end{Bmatrix} \quad (9)$$

where the functional dependence of E and H on z and t, $e^{j(\omega t - k_z z)}$, has been dropped for simplicity. The longitudinal components, E_z and H_z, and the transverse magnetic field in the y-direction, H_y, are nonzero, but negligible by a factor of λ/a. The transverse electric field in the x-direction is defined due to the linear polarization condition as $E_x = 0$.

The odd and even LP_{mn} modes are defined with a perpendicular electric field as

$$\vec{E}^{\perp}_{mn}(r,\phi) = \hat{y}AJ_m\left(\frac{X_{mn}r}{a}\right)\begin{cases}\cos(m\phi), & \text{(odd)}\\ \sin(m\phi), & \text{(even)}.\end{cases} \quad (10)$$

To create an orthonormal basis set, a normalization factor is calculated

$$N_{mn} = \int_0^a\int_0^{2\pi}\left(E^{\perp}_{mn}(r,\phi)\right)^2 r\, d\phi dr. \quad (11)$$

For LP_{0n} (HE_{1n}) modes, this normalization evaluates to

$$N_{0n} = A^2\pi a^2 J_1^2(X_{0n}) \quad (12)$$

and, for all other LP_{mn} modes, where $m \neq 0$, we have

$$N_{mn} = A^2\frac{\pi a^2}{2}J_{m-1}^2(X_{mn}). \quad (13)$$

With this factor

$$u_{mn} = E^{\perp}_{mn}/\sqrt{N_{mn}} \quad (14)$$

such that u_{mn} is a simple way to express the normalized mode.

III. Relationship Between Hybrid and LP_{mn} Modes

Any wave propagating in the corrugated metallic waveguide can be projected onto an orthonormal basis set of modes. Both the hybrid modes and the LP_{mn} modes form such a basis set.

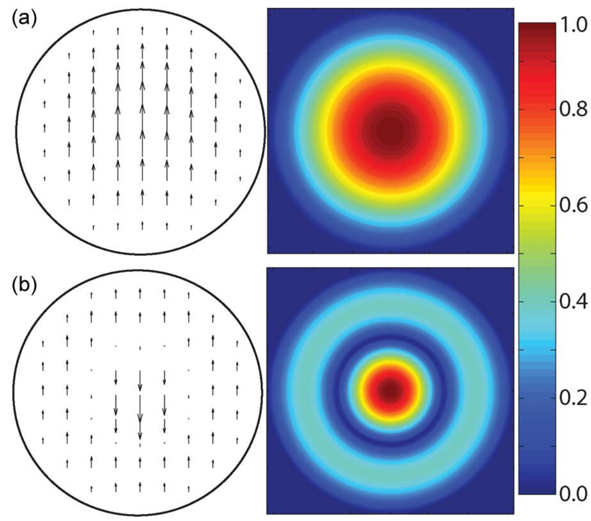

Fig. 2. Field vector and magnitude plots for: (a) $\mathrm{LP}_{01}/\mathrm{HE}_{11}$ and (b) $\mathrm{LP}_{02}/\mathrm{HE}_{12}$. (Amplitudes are normalized.)

TABLE I
SELECT LP MODES WITH CORRESPONDING DEGENERATE MODES

Mode	X_{mn}	Degenerate modes
LP_{01}	2.405	HE_{11}
$\mathrm{LP}_{11}^{(o)}$	3.832	TE_{01}, HE_{21}
$\mathrm{LP}_{11}^{(e)}$	3.832	TM_{02}, HE_{21}
LP_{21}	5.136	HE_{31}, EH_{12}
LP_{02}	5.520	HE_{12}
LP_{31}	6.380	HE_{41}, EH_{22}
$\mathrm{LP}_{12}^{(o)}$	7.016	TE_{02}, HE_{22}
$\mathrm{LP}_{12}^{(e)}$	7.016	TM_{03}, HE_{22}
LP_{22}	8.417	HE_{32}, EH_{13}
LP_{03}	8.653	HE_{13}
LP_{32}	9.761	HE_{42}, EH_{23}
$\mathrm{LP}_{13}^{(o)}$	10.17	TE_{03}, HE_{23}
$\mathrm{LP}_{13}^{(e)}$	10.17	TM_{04}, HE_{23}

Here, we indicate the relationships between these two basis sets and show how the LP_{mn} modes can be constructed from the hybrid mode basis set.

Fig. 2 illustrates the vector field and magnitude plots of the electric field for two common LP_{mn} modes. Note that the HE_{1n} modes are the same as the LP_{0n} modes. Therefore, the HE_{1n} notation will be kept in order to agree with the existing literature; this assignment is useful for discussing the fundamental HE_{11} mode.

LP_{mn} modes can be constructed through the addition of HE_{mn}, EH_{mn}, TE_{0n}, or TM_{0n} modes with the same propagation constants (degenerate modes). Table I lists these degenerate modes. Fig. 3 illustrates, for a few LP modes, how the addition of hybrid modes can form LP_{mn} modes. For all examples, the LP modes are constructed with a 1:1 power ratio of two hybrid modes, and the hybrid modes are rotated along the $\hat{z}$-axis to cancel $\hat{x}$-components of the electric fields. Cancellation of the $\hat{y}$-components could be achieved in a similar manner to form the $\hat{x}$-directed LP modes. A 180° phase shift between the hybrid modes corresponds to subtraction, as seen in Fig. 3(b). The first two examples, the LP_{11} modes, were previously described in [4]. Through the field vector plots, Fig. 3 demonstrates this relationship between LP modes and HE, EH, TE, and TM

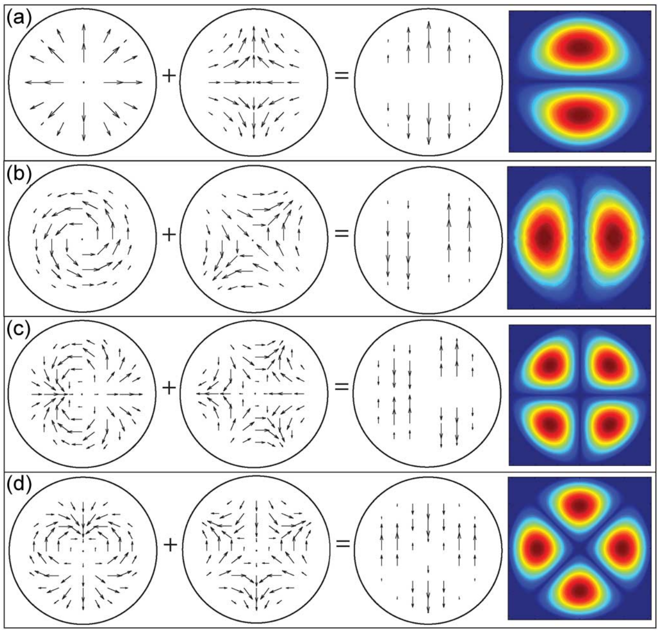

Fig. 3. Field vector plots demonstrating the construction of LP modes from TE, TM, and HE modes. The added modes have identical propagation constants. (a) TM_{02} + HE_{21} rotated 45° = $\mathrm{LP}_{11}^{(e)}$. (b) $-\mathrm{TE}_{01}$ + HE_{21} = $\mathrm{LP}_{11}^{(o)}$. (c) EH_{12} rotated -90° + HE_{31} rotated -90° = $\mathrm{LP}_{21}^{(e)}$. (d) EH_{12} rotated 180° + HE_{31} = $\mathrm{LP}_{21}^{(o)}$.

modes. For example, the $\mathrm{LP}_{11}^{(e)}$ mode can be constructed by adding the TM_{02} mode and the HE_{21} mode, rotated by 45°, as seen in Fig. 3(a). When adding these modes, the $\hat{x}$-components of the field cancel while the $\hat{y}$-components add, resulting in a $\hat{y}$-directed linearly polarized field. All three of these modes are characterized by the Bessel function zero $X_m = 3.832$ and, therefore, have the same beat wavelength as the HE_{11} mode. Since both sets of modes are basis sets, it is possible to use either set to describe a linearly polarized beam in a waveguide. However, it is necessary to account for HE, EH, TE, and TM modes that result in combinations (like those listed above) to preserve linear polarization. Due to this restriction, it is more convenient to consider the LP-mode basis set for analysis in corrugated cylindrical waveguides with linearly polarized experimental inputs.

IV. Gap Loss for Pure Mode Inputs

Most waveguide transmission lines are dominated by long, straight sections of waveguide which have negligible loss when $a/\lambda \gg 1$ [5]. However, a practical waveguide system must have waveguide gaps, bends, and switches in which the wave propagates a distance without a confining wall. Losses in these gaps often dominate the total loss of the line. Here, we calculate the power loss for an arbitrary LP_{mn} mode due to a gap in a straight waveguide. The exercise computes the field and mode amplitudes of a wave which radiates from the end of a transmitting waveguide through a gap consisting of free space and couples into a receiving waveguide after the gap. When the length of the gap L is equivalent to the diameter of the waveguide (that is, $L = 2a$), the gap geometry is an approximate 2-D model of a 90° miter bend in the waveguide, as shown in Fig. 4 [16]. Previously, the losses in a gap have been calculated for single-mode inputs consisting of HE, TE, or TM modes [18], [19].

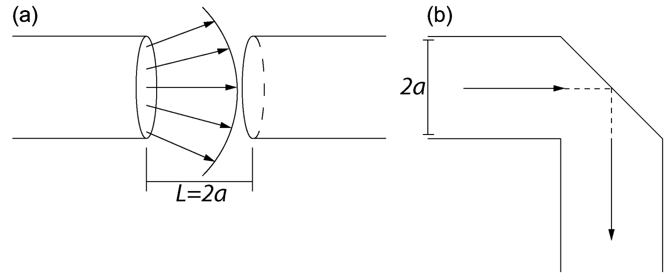

Fig. 4. (a) Radially symmetric gap with length $L = 2a$. (b) Miter bend with a radius of a that can be modeled using equivalent gap theory, as described in the text.

For LP_{mn} modes, the electric field in a gap is derived using the Fresnel diffraction integral, which is an approach similar to that in [14], such that

$$E_{g,mn}^{\perp}(r,\phi,z) = \frac{jk}{z} e^{j\frac{kr^2}{2z}} \int\int E_i(r',\phi') \times e^{j\frac{k}{2z}\left[r'^2 - 2rr'\cos(\phi-\phi')\right]} r' d\phi' dr' \quad (15)$$

where $E_i(r,\phi)$ defines the transverse electric field present at the end of the waveguide before the gap. This method is a Kirchhoff approximation, in which there are negligible reflections at the truncated apertures, since $a/\lambda \gg 1$ [20]. In the single-mode case, $E_i(r,\phi) = u_{mn}(r,\phi)$. Also, z is defined as the distance into the gap after the end of the waveguide. For an input consisting of a single normalized LP_{mn} odd mode, the electric field in the gap is

$$\vec{E}_{g,mn}^{\perp}(r,\phi,z) = \hat{y}\frac{j2\pi kA}{z\sqrt{N_{mn}}} e^{jm\frac{\pi}{2}} e^{j\frac{kr^2}{2z}} \cos(m\phi) \times \int_0^a J_m\left(\frac{X_n r'}{a}\right) J_m\left(\frac{krr'}{z}\right) e^{j\frac{kr'^2}{2z}} r' dr'. \quad (16)$$

The integral with respect to ϕ has been solved using methods discussed in [21], while the integral with respect to r' must be solved numerically. Note that LP_{mn} even modes result in the same $\vec{E}_{g,mn}^{\perp}(r,\phi,z)$ as (16) with $\cos(m\phi)$ replaced by $\sin(m\phi)$.

Power loss in a specific mode occurs in the gap for two reasons. First, as a result of diffraction, some of the power exiting the transmitting waveguide lies outside of the receiving waveguide at $r > a$ and is lost; this is called truncation loss. Second, there is power that enters the receiving waveguide but couples to secondary modes instead of the original input mode. For large a/λ, all of the modes produced in the receiving waveguide will propagate down the waveguide, the coupling to other modes results in additional power loss when considering the original mode. This is called mode conversion loss.

In the equivalent miter bend, shown in Fig. 4(b), the power lost due to truncation is trapped inside of the bend. The power is distributed into very high-order modes of the waveguide that do not propagate efficiently such that the power is dissipated through ohmic heating in long waveguide systems. The miter bend also suffers from mode conversion loss for the same reasons as in a gap. If the miter bend contains extensions of the waveguide into the bend, the loss is reduced to one half of that

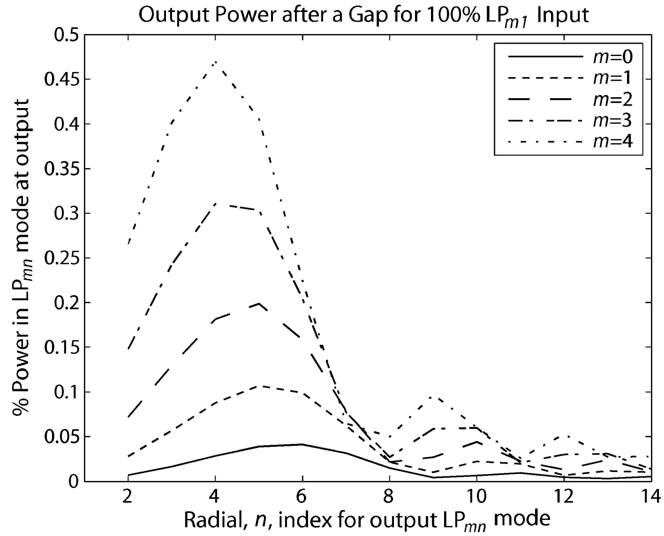

Fig. 5. Percent output of the power present in the LP_{mn} modes after a gap that results from a 100% LP_{m1} mode input, for $m = 0$–4. LP_{m1} mode power outputs (which are over 94%) have been cropped to emphasize higher order mode contents.

of the equivalent gap [16]. Since the gap model is azimuthally symmetric, there is no difference between the loss approximation and spurious modes for E- and H-plane miter bends with this method. Reference [22] discusses the spurious modes generated by optical mirrors in oversized waveguide in more detail.

For a/λ large, the power in the output port will consist primarily of power in the same mode (LP_{mn}) as was incident at the input port. Small amounts of power in other modes will also be present at the output port. These small amounts are illustrated for the case of LP_{m1} modes in Fig. 5. Fig. 5 shows the LP_{mn} mode content in the receiving guide due to a single LP_{m1} mode radiating from the transmitting guide through a gap of length $L = 2a$ and a system operating at 170 GHz with $a =$ 31.75 mm. Results are shown for cases with $m =$0–4. In these cases, over 94% of the power couples to the original input mode, less than 3% of the power is lost in the gap, and the rest of the power couples to higher order modes with the same azimuthal m index, as shown in the figure. Negligible reflections are assumed [20].

A particular input mode will only result in output modes of the same azimuthal symmetry. For example, the case of 100% HE_{11} (LP_{01} in Fig. 5) input results in 99.48% HE_{11} after the gap and 0.26% power lost in the gap. The remaining power goes into the HE_{1n} higher order modes, with the largest percentages in HE_{16} (0.041%) and HE_{15} (0.039%), while HE_{12} is the seventh largest mode with 0.007% of the total power. Also, consider an input of 100% $\mathrm{LP}_{11}^{(o)}$, which has an output of 98.68% $\mathrm{LP}_{11}^{(o)}$, 0.67% of power lost to the gap, and the remaining power coupled into higher order $\mathrm{LP}_{1n}^{(o)}$ modes. In each of these cases, the input power is either lost in the gap or couples into modes with the same azimuthal symmetry as the original input mode.

V. Gap Loss for Multiple-Mode Inputs

In the previous section, we considered a single mode at the input port of the gap. Here, we consider a multiple mode input. In this case, we must consider both the amplitudes of the modes and their phases. A multiple-mode input follows the same procedure as a single mode input. The gap loss is calculated using (15), where the input electric field is now defined as a summation of modes

$$E_i(r,\phi) = \sum_m \sum_n \sqrt{A_{mn}} e^{j\theta_{mn}} u_{mn}(r,\phi) \tag{17}$$

where A_{mn} and θ_{mn} indicate the relative power and phase of the input LP_{mn} modes. The output can also be expressed as a summation of each individual mode applied to (15) (as was done in (16) in the previous section) to yield

$$\vec{E}_g^{\perp}(r,\phi,L) = \sum_m \sum_n \sqrt{A_{mn}} e^{j\theta_{mn}} \vec{E}_{g,mn}^{\perp}(r,\phi,L). \tag{18}$$

The electric field in a gap for a multiple-mode input is simply the summation of the electric field in a gap due to each individual mode input. After summing, the modal powers in the waveguide after the gap are calculated in the same way as the single-mode case.

The phase difference between certain two-mode input mode combinations causes variations in the power loss and mode content after the gap. The output HE_{11} power due to an input consisting of the HE_{11} and HE_{12} modes has a significant dependence on input phase, as shown in Fig. 6(a) for gaps when $L = 2a$. Considering an input mode content of 98% HE_{11} and 2% HE_{12}, the power lost in HE_{11} ranges from 0.28% to 0.75%, corresponding to respective phase differences of 310° and 130°. The average loss in HE_{11} is 0.52%, the same value of loss as when HE_{11} is considered individually.

The dependence of power loss in a two-mode system on the phase difference between the modes is seen in any combination of modes that has the same azimuthal (m) symmetry. For example, an input consisting of HE_{11} and HE_{13} will also have an output dependent on the phase between the two modes. This effect is seen in Fig. 6(b). Though the average loss in HE_{11} is still 0.52%, with a 2% HE_{13} content, it may swing from 0.15% to 0.88%, depending on the input phase. This example treats modes of the same azimuthal symmetry (same m value). At the output port, a mode couples only to modes of the same azimuthal symmetry. Therefore, two modes of different azimuthal symmetry (different m values) will not interfere. For example, a two-mode input consisting of an HE_{11} (LP_{01}) mode ($m = 0$) and $\mathrm{LP}_{11}^{(o)}$ mode ($m = 1$) produces an output that has no dependence on the relative phase of the modes and will always result in a 0.52% loss in the HE_{11} mode power.

An input of three or more modes of the same azimuthal (m) symmetry will also result in a phase dependence. For example, an input consisting of HE_{11}, HE_{12}, and HE_{13}, will result in an output dependent on the phase relations between the modes. Results for varying values of higher order mode percentage and phases are shown in Fig. 7, where the x axis represents the total power in the combination of the HE_{12} and HE_{13} modes. The HE_{11} power loss is dependent on the phases of both modes as well as the percentage of power in each mode. A phase difference between HE_{11} and HE_{12} of 310° and HE_{13} of 120° causes the lowest possible power loss in HE_{11}, while phases of 130° and 300° in HE_{12} and HE_{13}, respectively, cause the largest possible power loss. Fig. 7 shows the curves corresponding to these two extreme phase combinations. Both the absolute highest and

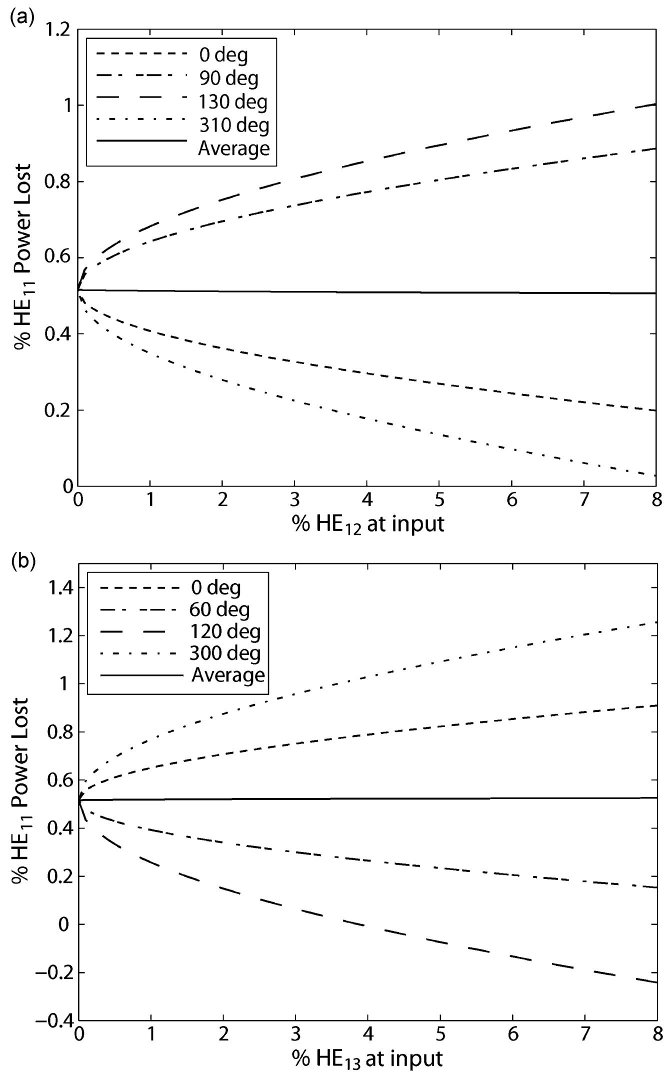

Fig. 6. For a two-mode input at 170 GHz with $a = 31.75$ mm and $L = 2a$, the percent of (a) HE_{12} or (b) HE_{13} present in the input mode mixture versus the percent loss in HE_{11} after the gap is plotted. Different phases of HE_{12} or HE_{13} have been chosen to show the full range of swing in the HE_{11} power loss. The average HE_{11} power loss is 0.52% for both cases.

lowest loss in HE_{11} power occur when 30% of the higher order mode content is in HE_{12}, and 70% is in HE_{13}. In this case, a 2% higher order mode content may cause a swing in lost HE_{11} output power from 0.08% to 0.95% a swing that is larger than the result from 2% in HE_{12} or HE_{13} individually.

VI. Constant of the Motion for Tilt and Offset

At the termination of a transmission line, the fields may be radiated from the end of the guide to an antenna or directly into space. If a single mode is propagating on the line, the mode will reach the end of the line such that the fields are centered on the waveguide. The radiation pattern at the end of the guide can be calculated in the near and far fields. For a single mode, the direction of propagation will always be centered on and parallel to the waveguide axis. When two or more modes propagate down the transmission line, it is no longer true that the field pattern is, in general, centered on the waveguide axis. The fields will radiate from the end of the waveguide, but the propagation angle will no longer, in general, be parallel to the waveguide axis. Here, we derive a simple new result for the propagation of two modes

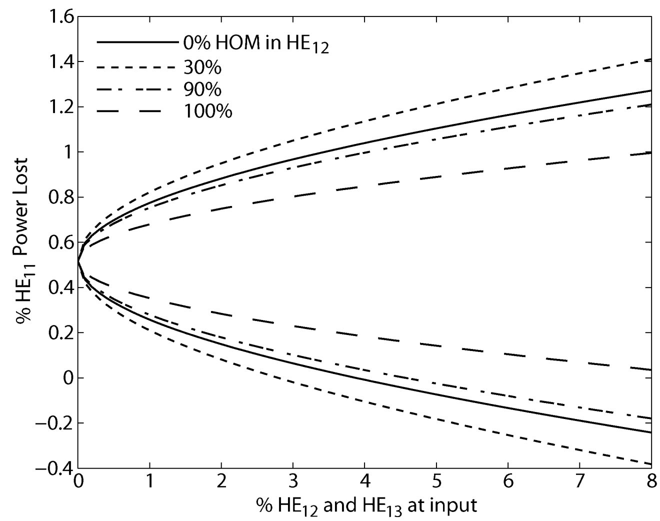

Fig. 7. Power loss in a gap for HE_{11} versus higher order mode content for a three-mode input. The higher order mode content is split between HE_{12} and HE_{13}, and the largest and smallest HE_{11} power loss (due to higher order mode phase) is plotted for each mode split. The system is at 170 GHz with $a = 31.75$ mm.

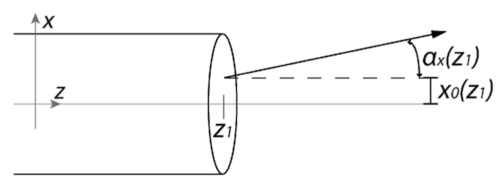

Fig. 8. Wave radiating from the end of a waveguide at z_1 has a centroid of power with an offset $x_0(z_1)$ and a tilt angle of propagation $\alpha_x(z_1)$ as defined here.

that shows a relationship between the tilt and offset at the terminus of a corrugated waveguide transmission line.

The problem is illustrated in Fig. 8, where the waveguide ends at a particular location of the z-axis, z_1. When a wave propagates outside of a waveguide, the centroid of power has a particular tilt angle $\alpha_{x,y}(z)$ and offset $x_0(z)$ and $y_0(z)$ from the center, as illustrated in Fig. 8. These two propagation parameters (tilt angle and offset) define the wave after the waveguide and quantify the centroid of power.

The offset and tilt angle of propagation are controlled by the mode content of the wave in the waveguide. A two-mode content is characterized by two parameters, the relative amplitude and phase difference between the modes. For a pure mode leaving a waveguide, the centroid of the mode power is always on axis $(x_0, y_0 = 0)$ and the mode has a constant flat phase front $(\alpha_{x,y} = 0)$. However, when two modes propagate, the power centroid will generally be off-center from the axis and the phase front will be tilted by an angle.

A conservation theorem expressing the relationship between tilt and offset for two propagating LP_{mn} modes is derived. For two modes, the electric field is defined as

$$E(x, y, z) = C_1(z)u_{m_1n_1}(x, y) + C_2(z)u_{m_2n_2}(x, y). \quad (19)$$

Here, C_p, where $p = 1, 2$, indicates the first or second mode of the system, is a complex variable indicating the amplitude and phase of the modes as

$$C_p(z) = \sqrt{A_p}e^{j(k_{z,p}z_1+\theta_p)}. \quad (20)$$

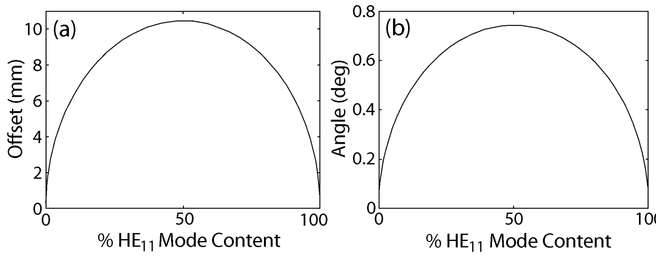

Fig. 9. Maximum: (a) offset and (b) tilt angle versus HE_{11} percent content [A_p in (20)] for a combination of HE_{11} and LP_{11} modes.

For the pth mode, A_p is the percentage of power in the mode, $k_{z,p}$ is the wavenumber in the $\hat{z}$-direction, and θ_p is the phase of the mode at $z_1 = 0$. Also, $u_{m_p n_p}(x, y)$ is the normalized field pattern of each mode as indicated in (14), with appropriate substitutions for r and ϕ to convert to the Cartesian coordinate system. The offset and propagation angle in the $\hat{x}$-direction are defined as

$$\begin{aligned} x_0(z_1) &= \langle x(z_1)\rangle \\ &= \iint E^*(x,y,z_1)xE(z,y,z_1)dxdy \qquad (21)\\ \alpha_x(z_1) &= \frac{\langle k_x(z_1)\rangle}{k} \\ &= \frac{-j}{k}\iint E^*(x,y,z_1)\frac{\partial E(x,y,z_1)}{\partial x}dxdy. \qquad (22)\end{aligned}$$

With the electric field defined for this problem, offset can be expressed as

$$\begin{aligned} x_0(z_1) = &\iint xC_1C_2^* u_{m_1n_1}u^*_{m_2n_2}dxdy \\ &+ \iint xC_1^*C_2u^*_{m_1n_1}u_{m_2n_2}dxdy \qquad (23)\end{aligned}$$

and reduced to

$$x_0(z_1) = 2\mathrm{Re}\left(C_1C_2^*\right)b_{12}. \qquad (24)$$

The propagation angle can also be expressed as

$$\begin{aligned}\alpha_x(z_1) = \frac{j}{k}\Bigg(&\iint C_1C_2^*u_{m_2n_2}\frac{\partial u_{m_1n_1}}{\partial x}dxdy \\ &- \iint C_1^*C_2u_{m_1n_1}\frac{\partial u_{m_2n_2}}{\partial x}dxdy\Bigg) \qquad (25)\end{aligned}$$

and reduced to

$$\alpha_x(z_1) = 2\mathrm{Im}\left(C_1C_2^*\right)d_{12}. \qquad (26)$$

The variables b_{12} and d_{12} are mode-specific integrals where

$$\begin{aligned} b_{12} &= \iint xu_{m_1n_1}u_{m_2n_2}dxdy \qquad (27)\\ d_{12} &= \frac{-1}{k}\iint u_{m_2n_2}\frac{\partial u_{m_1n_1}}{\partial x}dxdy. \qquad (28)\end{aligned}$$

The offset and angle in the $\hat{y}$-direction is similarly found with $x \to y$ and $y \to x$. Note that an angle and offset only occur for modes where $m_2 = m_1 \pm 1$; in all other cases, b_{12} and d_{12} evaluate to zero.

Due to the dependence on real and imaginary parts of the complex magnitudes, it is seen that the offset and angle change with the beating, or phase difference, between modes as the fields propagate. It is useful to define the offset and tilt as sinusoidal functions dependent on z_1 by using Euler's identity such that

$$\begin{aligned} x_0(z_1) &= x_{\max}\cos\left((\Delta k)z_1 + \theta_0\right) \qquad (29)\\ \alpha_x(z_1) &= -\alpha_{\max}\sin\left((\Delta k)z_1 + \theta_0\right). \qquad (30)\end{aligned}$$

In this case, $(\Delta k)z_1$ indicates the phase difference between the modes and θ_0 is the phase difference at $z = 0$ between the modes. The maximum possible offset and angle for a combination of two modes are defined as

$$\begin{aligned} x_{\max} &= 2b_{12}\left|C_1C_2^*\right| \qquad (31)\\ \alpha_{\max} &= 2d_{12}\left|C_1C_2^*\right|. \qquad (32)\end{aligned}$$

In addition, it can be inferred that $x_{\max}$ and $\alpha_{\max}$ occur when $C_1C_2^*$ is either purely real or purely imaginary, respectively.

Equations (29) and (30), together with (31) and (32), can be combined to form an expression for tilt and offset that is independent of location (z_1) on the transmission line, that is, the expression for tilt and offset may be combined to form a constant of the motion

$$\left(\frac{x_0(z_1)}{b_{12}}\right)^2 + \left(\frac{\alpha_x(z_1)}{d_{12}}\right)^2 = 4\left|C_1C_2^*\right|^2. \qquad (33)$$

The two governing parameters of the system are the percent split and phase difference between the two modes.

To illustrate this constant of the motion, we consider the common two mode combination of HE_{11} and $\mathrm{LP}_{11}^{(e)}$ modes. In this case, b_{12} and d_{12} are evaluated as

$$\begin{aligned} b_{12} &= \frac{\sqrt{2}}{a^2J_1(X_0)J_0(X_1)} \\ &\quad\times\int_0^a J_0\left(\frac{X_0r}{a}\right)J_1\left(\frac{X_1r}{a}\right)r^2dr \qquad (34)\\ d_{12} &= \frac{\lambda X_0X_1}{\sqrt{2}\pi a\left(X_1^2 - X_0^2\right)} \qquad (35)\end{aligned}$$

where $X_0 = 2.405$ and $X_1 = 3.832$, this gives $b_{12} = 0.329a$ and $d_{12} = 0.233\lambda/a$. For $a = 31.75$ mm and $\lambda = 1.76$ mm (170 GHz), these evaluate to $d_{12} = 0.74°$ and $b_{12} = 10.45$ mm. Fig. 9 shows the maximum angle and offset for an input of these two modes as defined in (31) and (32) versus the percent split between the two modes, the only variable parameter which will change the maximum angle and offset. Figs. 10 and 11 show the angle and offset due to an input with 80% HE_{11} and 20% LP_{11} or 90% HE_{11} and 10% LP_{11}, respectively, versus the phase difference between the modes, the second variable parameter. For these two modes, a phase difference of 2π corresponds to $z_1 = 5.07$ m. Due to interference effects, the power in the two modes propagates in the waveguide with sinusoidal oscillations in both tilt and offset, dependent on phase. By relation to the beat frequency between the two modes, the phase dependence can be quantified as the location in the waveguide where it is terminated and the wave is allowed to radiate into free space,

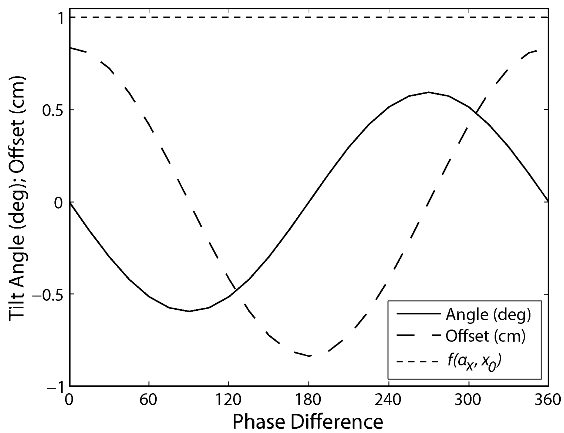

Fig. 10. Centroid offset and tilt angle for an input of 80% HE_{11} and 20% $\mathrm{LP}_{11}^{(e)}$ in a waveguide of radius $a = 31.75$ mm at 170 GHz. $f(\alpha_x, x_0)$ plots (36). A 2π phase difference corresponds to $z_1 = 5.07$ m.

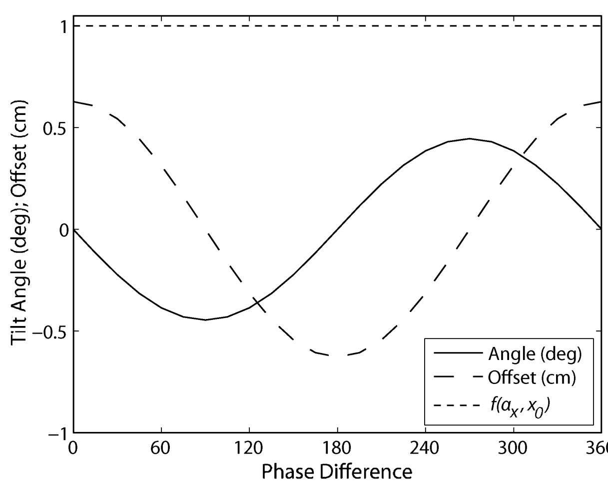

Fig. 11. Centroid offset and tilt angle for an input of 90% HE_{11} and 10% $\mathrm{LP}_{11}^{(e)}$ in a waveguide of radius $a = 31.75$ mm at 170 GHz. $f(\alpha_x, x_0)$ plots (36). A 2π phase difference corresponds to $z_1 = 5.07$ m.

$\theta = (\Delta k)z_1 + \theta_0$. Fig. 10 has a larger split between the mode contents than Fig. 11 does, causing a larger amplitude of offset and angle oscillations. In both figures, the oscillations are out of phase by 90° and combine [using (33)] to form a constant of the motion. In both figures, we calculate $f(\alpha_x, x_0)$, where

$$f(\alpha_x, x_0) = \frac{1}{4\left|C_1 C_2^*\right|^2}\left[\left(\frac{x_0(z_1)}{b_{12}}\right)^2 + \left(\frac{\alpha_x(z_1)}{d_{12}}\right)^2\right] \quad (36)$$

and show that it is unity for all phases. Other percent splits between HE_{11} and LP_{11} will behave in the same pattern. In addition, other two-mode combinations that result in a centroid offset will behave similarly, i.e., modes that vary by one azimuthal index will follow the same pattern as the HE_{11} and LP_{11} combination illustrated here.

VII. Discussion and Conclusion

We have shown that the LP_{mn} modes form a convenient basis set for linearly polarized waves that are transmitted in large-diameter corrugated metallic waveguides with quarter-wave corrugations. The LP_{mn} modes may also be used to quantify the effects of higher order modes in overmoded transmission lines. Applying this basis set to calculate the loss due to a gap in the waveguide for a pure mode input provides an assessment of the higher order modes of the same azimuthal symmetry generated in a gap. An LP_{mn} mode at the input port of a gap generates higher order modes at the output port with the same azimuthal symmetry (same m value). With a multiple mode input, the azimuthal symmetry of the problem reduces the complexity of analysis. For example, when considering the loss in a gap due to two modes, inputs which consist of HE_{11} and a higher order HE_{1n} mode will generate a phase dependence on HE_{11} loss. However, input with HE_{11} and LP_{mn} modes with $m > 0$ have a loss that is not dependent on phase. The phase between HE_{1n} modes causes a swing in the HE_{11} power loss which increases with increasing higher order mode content, but the average loss in HE_{11} mode power over input higher order mode phases is not dependent on the amplitude of the higher order mode content.

The constant of motion for tilt and offset of a wave exiting a waveguide is useful in quantifying the effect of higher order modes on transmission lines. This constant of motion relates the tilt and offset due to a particular two mode combination in the waveguide. For an angle and offset to occur, the two modes must be related such that the azimuthal indexes vary by one, $m_2 = m_1 \pm 1$. The phase difference between modes modifies the split between centroid offset and propagation angle, but does not affect the constant of motion between the two parameters.

References

[1] P. J. Clarricoats and A. D. Olver, "Low attenuation in corrugated circular waveguides," *Electron. Lett.*, vol. 9, no. 16, pp. 376–377, Aug. 1973.

[2] A. Cavallo, J. Doane, and R. Cutler, "Low-loss broadband multimode corrugated waveguide performance," *Rev. Sci. Instr.*, vol. 81, no. 9, pp. 2396–2400, Sep. 1990.

[3] E. Marcatili, "Hollow metallic and dielectric waveguides for long distance optical transmission and lasers," *Bell Syst. Tech. J.*, vol. 43, pp. 1783–1809, 1964.

[4] P. J. Clarricoats and R. D. Elliot, "Multimode corrugated waveguide feed for monopulse radar," *Proc. IEEE*, vol. 128, no. 2, pp. 102–110, Apr. 1981.

[5] J. L. Doane, "Propagation and mode coupling in corrugated and smooth-wall circular waveguides," in *Infrared and Millimeter Waves*, K. J. Button, Ed. New York: Academic, 1985, vol. 13, ch. 5.

[6] A. D. Olver, P. J. Clarricoats, and S. L. Chong, "Experimental determination of attenuation in corrugated circular waveguides," *Electron. Lett.*, vol. 9, no. 18, pp. 424–426, Sep. 1973.

[7] M. K. Thumm and W. Kasparek, "Passive high-power microwave components," *IEEE Trans. Plasma Sci.*, vol. 30, no. 3, pp. 755–786, Jun. 2002.

[8] C. Dragone, "Attenuation and radiation characteristics of the HE_{11}-mode," *IEEE Trans. Microw. Theory Tech.*, vol. MTT-28, no. 7, pp. 704–710, Jul. 1980.

[9] J. P. Crenn and C. Charollais, "Propagation and radiation characteristics of the circular electric, circular magnetic, and hybrid waveguide modes," *Int. J. Infrared Millim. Waves*, vol. 17, no. 9, pp. 1475–1506, Sep. 1996.

[10] M. A. Henderson, B. Beckett, C. Darbos, N. Kobayashi, G. Saibene, F. Albajar, and T. Bonicelli, "A revised ITER EC system baseline design proposal," in *Proc. 15th Joint Workshop Electron Cyclotron Emission and Electron Cyclotron Resonance Heating*, J. Lohr, Ed., 2009, pp. 453–484.

[11] R. A. Olstad, J. L. Doane, and C. P. Moeller, "Considerations in selection of ECH transmission line waveguide diameter for ITER," in *Proc. 3rd JAEA Tech. Meeting ECRH Phys. Tech. ITER, J. Phys. Conf. Ser.*, 2005, vol. 25, pp. 166–171.

[12] R. J. Abrams, "Coupling losses in hollow waveguide laser resonators," *IEEE J. Quantum Electron.*, vol. QE-8, no. 11, pp. 838–843, Nov. 1972.

[13] K. Ohkubo, S. Kubo, H. Idei, M. Sato, T. Shimozuma, and Y. Takita, "Coupling of tilting Gaussian beam with hybrid mode in the corrugated waveguide," *Int. J. Infrared Millim. Waves*, vol. 18, no. 1, pp. 23–41, Jan. 1997.

[14] J. J. Degnan, "Waveguide laser mode patterns in the near and far field," *Appl. Opt.*, vol. 12, no. 5, pp. 1026–1030, May 1973.

[15] J. J. Degnan, "The waveguide laser: A review," *Appl. Phys.*, vol. 11, no. 1, pp. 1–33, Sep. 1976.

[16] E. Marcatili, "Miter elbow for circular electric modes," in *Proc. Symp. Quasi-Opt.*, Brooklyn, NY, Jun. 8–10, 1964, pp. 535–542.

[17] A. Yariv, *Optical Electronics*. Philadelphia, PA: Saunders College, 1991.

[18] J. L. Doane and C. P. Moeller, " HE_{11} mitre bends and gaps in a circular corrugated waveguide," *Int. J. Electron.*, vol. 77, pp. 489–509, Oct. 1994.

[19] D. Wagner, M. Thumm, K. Kasparek, G. A. Muller, and O. Braz, "Prediction of TE-, TM-, and hybrid-mode transmission losses in gaps of oversized waveguides using a scattering matrix code," *Int. J. Infrared Millim. Waves*, vol. 17, no. 6, pp. 1071–1081, Jun. 1996.

[20] L. A. Weinstein, *The Theory of Diffraction and the Factorization Method (Generalized Weiner-Hopf Technique)*, ser. Golem series in electromagnetics. Boulder, CO: Golem, 1969, vol. 3.

[21] A. G. Fox and T. Li, "Resonant modes in a maser interferometer," *Bell Syst. Tech. J.*, vol. 40, no. 2, pp. 453–488, 1961.

[22] B. Z. Katsenelenbaum, "Diffraction on plane mirror in broad waveguide junction," *Radio Eng. Electron. Phys.*, vol. 8, pp. 1098–1106, 1963.

Elizabeth J. Kowalski (S'10) received the B.S. degree in electrical engineering (with honors) from the Pennsylvania State University, University Park, in 2008, and the S.M. degree in electrical engineering from the Massachusetts Institute of Technology, Cambridge, in 2010, where she is currently working toward the Ph.D. degree.

She is a Graduate Research Assistant with the Waves and Beams Division at the Massachusetts Institute of Technology Plasma Science and Fusion Center. Her research interests include high-power, high-frequency vacuum electronic devices.

Ms. Kowalski was the recipient of the Department of Energy Office of Science Fellowship for 2010.

David S. Tax (S'09) received the B.Eng. degree in electrical engineering from Dalhousie University, Halifax, NS, Canada, in 2005, and the M.S. degree at the Massachusetts Institute of Technology, Cambridge, in 2008, where he is currently working toward the Ph.D. degree. His master's work focused on mode conversion losses in overmoded millimeter wave transmission lines.

He is currently with the Plasma Science and Fusion Center, Massachusetts Institute of Technology, with the Waves and Beams Division. His current research focus involves the development of high-power, multifrequency gyrotrons and the study of the efficiency of such devices.

Michael A. Shapiro (M'09) received the Ph.D. degree in radio physics from the University of Gorky, Gorky, Russia in 1990.

Since 1995, he has been with the Plasma Science and Fusion Center, Massachusetts Institute of Technology, Cambridge, where he is currently Head of the Gyrotron Research Group. His research interests include vacuum microwave electron devices, high-power gyrotrons, dynamic nuclear polarization spectroscopy, high-gradient linear accelerators, quasi-optical millimeter-wave components, and photonic bandgap structures and metamaterials.

Jagadishwar R. Sirigiri (S'98–M'03) received the B.Tech. degree in electronics engineering from the Institute of Technology, Banaras Hindu University, India, in 1996, and the S.M. and Ph.D. degrees in electrical engineering and computer science from the Massachusetts Institute of Technology, Cambridge, in 2000 and 2003, respectively.

He was a Senior Hardware Engineer with Wipro Infotech in India from 1996 to 1998, where he was involved in the development of multimedia products including hardware-based videoconferencing solutions. Since 2005, he has been a Research Scientist with the Massachusetts Institute of Technology's Plasma Science and Fusion Center, where he leads the experimental program in the Waves and Beams Division. He demonstrated the first vacuum electron device with a photonic bandgap resonator to achieve single-mode operation in a highly overmoded device at 140 GHz. His primary research areas include research and development of megawatt class gyrotron systems for heating of fusion plasmas, millimeter-wave (mm-wave) and sub-mm-wave gyrotrons for dynamic nuclear polarization in NMR experiments, slow-wave and fast-wave amplifiers in the W-band for radar and communication experiments, and high gradient accelerators.

Dr. Sirigiri was the guest editor of the 12th Special Issue on High Power Microwaves of the IEEE TRANSACTIONS ON PLASMA SCIENCE in 2008.

Richard J. Temkin (M'87–SM'92–F'94) received the B.A. degree in physics from Harvard College, Cambridge, MA, and the Ph.D. degree in physics from the Massachusetts Institute of Technology, Cambridge.

From 1971 to 1974, he was a Postdoctoral Research Fellow with the Division of Engineering and Applied Physics, Harvard University. Since 1974, he has been with the Massachusetts Institute of Technology, first with the Francis Bitter National Magnet Laboratory and later with the Plasma Science and Fusion Center (PSFC) and the Department of Physics. He currently serves as a Senior Scientist in the Physics Department, as Associate Director of the PSFC, and Head of the Waves and Beams Division, PSFC. His research interests include novel vacuum electron devices such as the gyrotron and free electron laser, advanced high-gradient electron accelerators, overmoded waveguides and antennas at millimeter/THz wavelengths, high-power microwave sources and their applications, plasma heating, and dynamic nuclear polarization/NMR. He has authored or coauthored over 200 published journal articles and book chapters and has been the editor of six books and conference proceedings.

Dr. Temkin is a Fellow of the American Physical Society and The Institute of Physics, London, U.K. He was the recipient of the Kenneth J. Button Prize and Medal of The Institute of Physics, London and the Robert L. Woods Award of the Department of Defense for Excellence in Vacuum Electronics research.

Timothy S. Bigelow , photograph and biography not available at the time of publication.

David A. Rasmussen , photograph and biography not available at the time of publication.